Available online at www.sciencedirect.com

SciVerse ScienceDirect

Acta Materialia 60 (2012) 5233–5244

Acta MATERIALIA

www.elsevier.com/locate/actamat

A probabilistic crystal plasticity model for modeling grain shape effects based on slip geometry

Shang Sun [a], Veera Sundararaghavan [b,*]

[a] Department of Naval Architecture and Marine Engineering, University of Michigan, 2600 Draper Dr., Ann Arbor, MI 48109, USA
[b] Department of Aerospace Engineering, University of Michigan, 3025 FXB Building, 1320 Beal Ave, Ann Arbor, MI 48109, USA

Received 21 March 2012; received in revised form 29 May 2012; accepted 30 May 2012
Available online 24 July 2012

Abstract

A new statistical theory is introduced that takes into account the coupling between grain size, shape and crystallographic texture during deformation of polycrystalline microstructures. A "grain size orientation distribution function" (GSODF) is used to encode the probability density of finding a grain size D along a direction (given by unit vector $\boldsymbol{n}$) in grains with orientation $\boldsymbol{g}$. The GSODF is sampled from the input microstructure and is represented in a finite element mesh. During elastoplastic deformation, the evolution of grain size D (in direction θ) and the orientation g is tracked by directly updating the GSODF probabilities using a Lagrangian probability update scheme. The effect of grain shape (e.g. in high aspect ratio grains) is modeled by including the apparent grain size as seen by various different active slip systems in the grain within the constitutive law for the slip system resistance. The prediction of texture and strains achieved by the statistical approach is compared to Taylor aggregate and finite element deformation analysis of a planar polycrystalline microstructure. The role of grain shape and size in determining plastic response is investigated and a new adaptive GSODF model for modeling microstructures with multimodal grain shapes is proposed.

Keywords: Plastic deformation; Texture; Finite element analysis; Simulation; Theory

1. Introduction

Efficient microscale modeling tools are needed to compute microstructure-dependent properties of advanced structural alloys used in aerospace, naval and automotive applications. Microstructural features such as texture, grain size and shape distribution plays an important role in determining the yield strength of such alloys. Efficient models that couple the effect of these statistical features are important for establishing the means to optimize these materials and enhance performance of critical hardware components [1]. Hall and Petch [2,3] established the well-known relationship that relates macroscopic yield strength of a polycrystalline material to the inverse square root of the average grain size (d). Traditional crystal plasticity models [4,5] were developed largely without a connection to grain size and shape effects. Incorporation of grain size effect into constitutive models for single slip began in 1962 with Armstrong [6], who modified the Hall–Petch equation to correspond to the flow stress on a slip system (the "micro-Hall–Petch relation"). The interrelationship between grain size and texture was not considered until 1983, when Weng [7] employed the mean grain size in the equation for slip system resistance through the micro-Hall–Petch relation. A significant body of work has incorporated grain-size effect within crystal plasticity simulations using either the micro-Hall–Petch relation [8,9] or using gradient theories [10–13]. However, these models only considered grain size effects in equiaxed grains and not the effect of grain shape pertaining to non-equiaxed grains, high aspect ratio grains and multimodal grain size distributions.

Some attempts have been made in the past to consider the effect of grain shape on anisotropy in yield strength [14–16]. Bunge et al. [14] incorporated a micro-Hall–Petch relationship within the Taylor model [17] by modeling

* Corresponding author. Tel.: +1 734 615 7242.
E-mail address: veeras@umich.edu (V. Sundararaghavan).

1359-6454/$36.00 © 2012 Acta Materialia Inc. Published by Elsevier Ltd. All rights reserved.
http://dx.doi.org/10.1016/j.actamat.2012.05.039

individual grains as ellipsoids and by computing the apparent grain size along each active slip direction. The change in shape of the grains during deformation was accounted for, but the work did not incorporate texture evolution. The recent model of Fromm et al. [18] coupled grain size distribution and texture within a viscoplastic model and found large yield stress anisotropy due to the coupling between grain size distribution and crystallographic texture. However, this study did not factor in the effect of grain shape, i.e. the effect of differences in apparent grain sizes along various slip directions in elongated grains and the evolution of the grain sizes during deformation (e.g. flattening of grains during rolling processes). The primary purpose of this paper is to combine the idea of Bunge et al. [14] within the statistical model of Fromm et al. [18] in order to achieve a more complete coupling between grain orientation and grain size/shape effects into crystal plasticity. The new statistical modeling approach introduced here can be used to evolve the grain size and orientation distribution function (GSODF) during loading processes. Our aim is to develop an extremely efficient approach that can be used to perform simulations in a fraction of the time of a finite element (FE) or a Taylor aggregate model.

The GSODF, defined as $\mathscr{F}(\boldsymbol{r},\boldsymbol{g})$ in this work, gives the probability density of finding a grain of orientation $\boldsymbol{g}$ in the microstructure with a grain size $|\boldsymbol{r}|$in the direction $\frac{\boldsymbol{r}}{|\boldsymbol{r}|}$. In our previous work [19], we introduced an FE approach for representing and evolving microstructure probability density functions during deformation. Using this approach, the GSODF is described as a field variable over interconnected FE meshes in the $\boldsymbol{r}$ space and $\boldsymbol{g}$ space (the fundamental region of crystal orientations). As the microstructure evolves, the crystallographic reorientations and shape changes of grains are captured by updating the GSODF field over these meshes. A total Lagrangian algorithm has been developed that allows evolution of probability densities while satisfying basic normalization and crystallographic symmetry constraints. For validation of the approach, the predictions of texture and strains achieved by the GSODF approach are compared to a Taylor aggregate model and an FE model of a planar polycrystalline microstructure that uses the micro-Hall–Petch relationship. Finally, the use of adaptive GSODFs for determining the overall stress–strain response is investigated in the case of two-dimensional (2-D) microstructures with bimodal grain size distributions.

2. Representation of the GSODF

The GSODF, $\mathscr{F}(\boldsymbol{r},\boldsymbol{g})$, gives the probability density of finding a grain of orientation $\boldsymbol{g}$ in a microstructure with a grain size $|\boldsymbol{r}|$in the direction $\frac{\boldsymbol{r}}{|\boldsymbol{r}|}$. The descriptor inherently includes information about lower-order descriptors such as (i) the orientation distribution function (ODF, $\mathscr{A}(\boldsymbol{g})$), which gives the probability density of finding an orientation $\boldsymbol{g}$ in the microstructure, and (ii) the orientation-specific grain size distribution function (GSDF, $\mathscr{P}(\boldsymbol{r}|\boldsymbol{g})$), which gives the probability density of finding grain size $|\boldsymbol{r}|$in the direction $\frac{\boldsymbol{r}}{|\boldsymbol{r}|}$, given that only grains with orientation $\boldsymbol{g}$ are sampled. This can be seen from the Bayesian relationship: $\mathscr{F}(\boldsymbol{r},\boldsymbol{g}) = \mathscr{P}(\boldsymbol{r}|\boldsymbol{g})\mathscr{A}(\boldsymbol{g})$. The GSODF satisfies the following conservation equations at all times during deformation:

$$\int \mathscr{P}(\boldsymbol{r}|\boldsymbol{g})d\boldsymbol{r} = 1, \ (\text{with } \mathscr{P}(\boldsymbol{r}|\boldsymbol{g}) \geqslant 0) \tag{1}$$

$$\int \mathscr{A}(\boldsymbol{g})d\boldsymbol{g} = 1 \ (\text{with } \mathscr{A}(\boldsymbol{g}) \geqslant 0) \tag{2}$$

where $d\boldsymbol{g}$ is a differential volume element (the invariant measure) of the orientation space. In addition to the above constraints, the orientation space corresponding to all possible $\boldsymbol{g}$'s must satisfy the crystallographic symmetries of the chosen system (face-centered cubic (fcc), hexagonal close-packed (hcp) etc.).

The complete orientation space of a polycrystal can be reduced to a smaller subset, called the fundamental region, as a consequence of crystal symmetries. Within the fundamental region, each crystal orientation is represented uniquely by the coordinate $\boldsymbol{g}$, the parametrization for the rotation (e.g. Euler angles, the Rodrigues vector). The ODF ($\mathscr{A}(\boldsymbol{g})$) can be represented as a probability density function over the fundamental region of orientation space.

For simplicity, consider planar polycrystals characterized by a 2-D rotation $\boldsymbol{R}$ that relates the local crystal lattice frame to the reference sample frame. A parametrization of the associated rotation group is

$$\boldsymbol{R} = \boldsymbol{I}cos(g) - \boldsymbol{E}sin(g) \tag{3}$$

where g is the angle between the crystal and sample axes, $\boldsymbol{E}$ is the 2-D alternator ($E_{11} = E_{22} = 0$, $E_{12} = -E_{21} = 1$) and $\boldsymbol{I}$ is the identity tensor. A general planar crystal with symmetry under rotations through π is considered here. Under the symmetry, crystal orientations can be described uniquely by parameters drawn from a simply connected fundamental region $[a, a+\pi)$. For convenience, we restrict the choice of fundamental regions to the interval closest to the origin $(-\pi/2, \pi/2)$. Due to symmetry, the orientation $\pi/2$ is exactly the same as the orientation $-\pi/2$.

In this work, an FE mesh is used to model the fundamental region and the ODF is defined at the nodal points of this mesh [20,21]. The probability values between nodal points are obtained as a result of interpolation using FE shape functions. The symmetry constraint on the ODF is enforced by using periodic boundary conditions in the FE mesh wherein the node at $g = \pi/2$ is considered a dependent node with field values updated using values at $g = -\pi/2$. The FE grid for the fundamental region will be referred to as M_g. Note that alternate approaches based on spectral expansions [22,23] of ODFs are also possible, although these are global representations (compared to FEs that have local basis functions that can efficiently capture sharp textures).

The orientation-specific grain size distribution function ($\mathscr{P}(\boldsymbol{r}|\boldsymbol{g})$) is also represented over an FE grid (named mesh $M_{r|g}$). For a 2-D microstructure, the region $\boldsymbol{r}$ can be taken

to be a semi-circle spanning sampling directions from $-\pi/2$ to $+\pi/2$. The radius of the semi-circle is taken to be equal to the maximum possible grain size sampled from the microstructure. The GSODF, $\mathscr{F}(\boldsymbol{r},\boldsymbol{g})$, is represented using meshes $M_{r|g}$ defined at every node point in the fundamental region (mesh M_g). The approach is illustrated in Fig. 1 for a planar microstructure. The GSDF $\mathscr{P}(\boldsymbol{r}|\boldsymbol{g})$ is described over mesh $M_{r|g}$ and the ODF $\mathscr{A}(\boldsymbol{g})$ is described over mesh M_g. From this representation, GSODF can be retrieved using the Bayesian relationship: $\mathscr{F}(\boldsymbol{r},\boldsymbol{g}) = \mathscr{P}(\boldsymbol{r}|\boldsymbol{g})\mathscr{A}(\boldsymbol{g})$. Grain size distribution can be assessed based on ASTM grain size standard E-112 using the Heyn intercept method [24]. In this method, parallel lines at different orientation angles are superposed over the microstructure. The histogram of the intercept length distribution, i.e. intercept length vs. number of test lines possessing the intercept length, is normalized to obtain the grain size distribution function (see Fig. 3, Section 6).

3. Probability update in FE spaces

The probabilities are evolved from time $t = 0$ from an initial GSODF that satisfies the conservation equations Eqs. (1) and (2) using a Lagrangian FE approach [19,25]. The initial orientation $\boldsymbol{g}_o$ of a crystal reorients during deformation and maps to a new orientation $\boldsymbol{g}_t$ at time t. Simultaneously, the FE mesh of fundamental region M_g deforms, with nodes located at $\boldsymbol{g}_o$ moving to new locations $\boldsymbol{g}_t$. We assume that the mapping from $\boldsymbol{g}_o$ to $\boldsymbol{g}_t$ is invertible.

The ODF $\mathscr{A}(\boldsymbol{g}_t)$ represents the probability density of crystals with orientation $\boldsymbol{g}_t$ at time t. The evolution of ODF is given by the conservation Eq. (2) as:

$$\int \mathscr{A}(\boldsymbol{g}_o, t=0)d\boldsymbol{g}_o = \int \mathscr{A}(\boldsymbol{g}_t)d\boldsymbol{g}_t = 1 \tag{4}$$

where $d\boldsymbol{g}_o$ represents the volume element in the undeformed (initial) ODF mesh (M_{g_o}), which becomes volume element

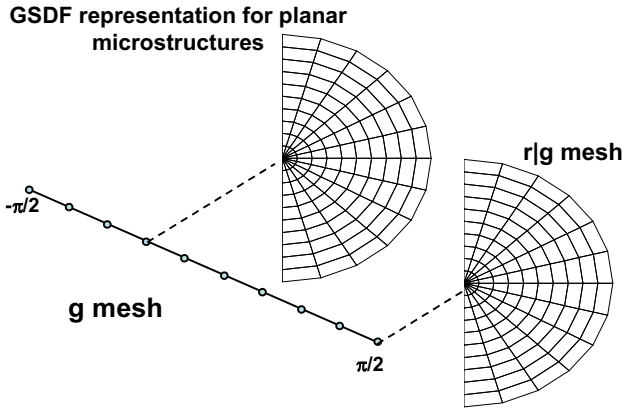

Fig. 1. The GSODF, $\mathscr{F}(\boldsymbol{r},\boldsymbol{g})$, is represented in the mesh structure shown here. The semi-circle mesh $M_{r|g}$ is defined for every node point in another FE discretized fundamental region (mesh M_g). The approach is illustrated for a planar microstructure (with the fundamental region mesh M_g being a line between $-\pi/2$ and $\pi/2$). The GSDF $\mathscr{P}(\boldsymbol{r}|\boldsymbol{g})$ is described over mesh $M_{r|g}$ and the ODF $\mathscr{A}(\boldsymbol{g})$ is described over mesh M_g.

$d\boldsymbol{g}_t$ at time t. A Jacobian $J(\boldsymbol{g}_o,t) = \det(\boldsymbol{G})$ gives the ratio of elemental volumes such that $d\boldsymbol{g}_t = J(\boldsymbol{g}_o,t)d\boldsymbol{g}_o$, where $\boldsymbol{G}$ is the reorientation gradient given as $\boldsymbol{G}(\boldsymbol{g}_o,t) = \frac{\partial \boldsymbol{g}_t}{\partial \boldsymbol{g}_o}$. Using the Jacobian, a map of the current mesh (at time t) to the reference mesh (at $t = 0$) can be made:

$$\int (\mathscr{A}(\boldsymbol{g}_o, t=0) - \widehat{\mathscr{A}}(\boldsymbol{g}_o,t)J(\boldsymbol{g}_o,t))d\boldsymbol{g}_o = 0 \tag{5}$$

The quantity written as $\widehat{\mathscr{A}}(\boldsymbol{g}_o,t)$ is the volume density $\mathscr{A}(\boldsymbol{g}_t)$ plotted over the corresponding orientation ($\boldsymbol{g}_o$) in the initial mesh. Thus, $\widehat{\mathscr{A}}(\boldsymbol{g}_o,t)$ gives the Lagrangian representation of the current ODF in the initial mesh M_{g_o}. If the integrand is continuous, a localized relationship of the following form can be used to update the ODF at any time t:

$$\widehat{\mathscr{A}}(\boldsymbol{g}_o,t)J(\boldsymbol{g}_o,t) = \mathscr{A}(\boldsymbol{g}_o, t=0) \tag{6}$$

Fig. 2 gives an idea of how the approach works for a 1-D fundamental region that is represented using two-noded FEs with linear interpolation. Here, the Jacobian is simply the ratio of element lengths, i.e. current length divided by the initial length. If the element length decreases over time, the probability density has to increase based on Eq. (6) to maintain normalization of the ODF. Note that the integrand in Eq. (5) needs to be continuous for the localization relationship to be valid. Thus, it is implied that $J(\boldsymbol{g}_o,\ t)$ needs to be continuous. For computing $J(\boldsymbol{g}_o,\ t)$, a reorientation velocity $\boldsymbol{v} = \frac{\partial \boldsymbol{g}_t}{\partial t}$ is calculated from the elasto-plastic constitutive model (described later). Consequently, $\boldsymbol{v}$ needs to be continuously differentiable (at least piecewise) in the fundamental region. This is a restriction on the constitutive model. Note that the differentiability of $\boldsymbol{v}$ will also ensure invertibility of the map from $\boldsymbol{g}_o$ to $\boldsymbol{g}_t$.

A similar approach can be used to update the probability density $\mathscr{P}$ in the mesh $M_{r|g}$. The evolution of probability density $\mathscr{P}$ is given by the conservation equation, Eq. (2), as:

$$\int (\widehat{\mathscr{P}}(\boldsymbol{r}_o,t|\boldsymbol{g})J(\boldsymbol{r}_o,t|\boldsymbol{g}) - \mathscr{P}(\boldsymbol{r}_o,t=0|\boldsymbol{g}))d\boldsymbol{r}_{o_g} = 0 \tag{7}$$

where $d\boldsymbol{r}_{o_g}$ represents the volume element in the undeformed (initial) mesh ($M_{r|g}$) and $J(\boldsymbol{r}_o,t|\boldsymbol{g}) = \det\left(\frac{\partial \boldsymbol{r}_t}{\partial \boldsymbol{r}_o}(\boldsymbol{g})\right)$ is the Jacobian for a volume element corresponding to grain size $\boldsymbol{r}_o$. A localized relation of the following form is used to compute the probability density at time t:

$$\widehat{\mathscr{P}}(\boldsymbol{r}_o,t|\boldsymbol{g})J(\boldsymbol{r}_o,t|\boldsymbol{g}) = \mathscr{P}(\boldsymbol{r}_o,t=0|\boldsymbol{g}) \tag{8}$$

4. Constitutive modeling

We employ the (now) classical single-crystal plasticity theory [26] based on the notion that plastic flow takes place through slip on prescribed slip systems. For a material with $\alpha = 1,\ldots,N$ slip systems defined by ortho-normal vector pairs $\left(\boldsymbol{m}_0^\alpha, \boldsymbol{n}_0^\alpha\right)$, denoting the slip direction and slip plane normal respectively at time $t = 0$, the constitutive equations relate the following basic fields (all quantities expressed in

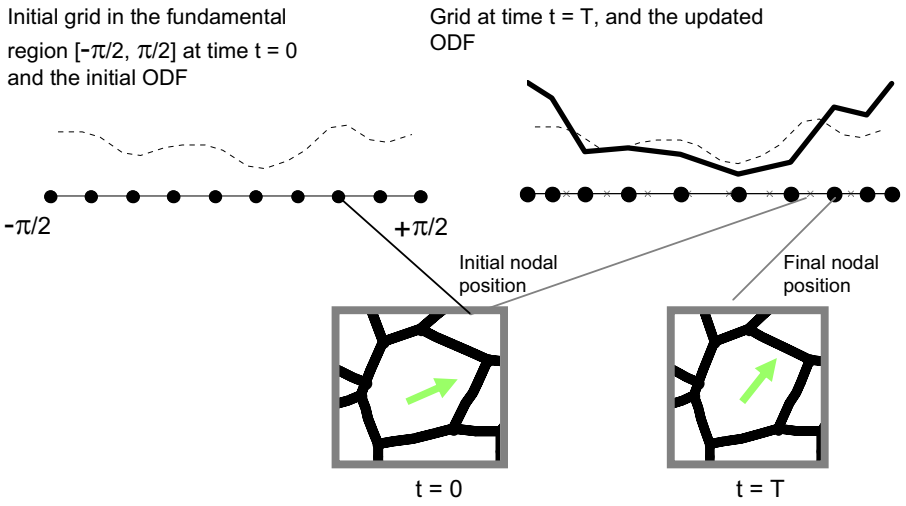

Fig. 2. Probability update scheme in FE space: during deformation, the nodal points ($\boldsymbol{g}$) of the FE mesh are moved to reflect reorientation ($\Delta\boldsymbol{g}$) of crystals. The new ODF is obtained using Eq. (6), which ensures that the normalization constraint (Eq. (4)) is met in the reoriented mesh.

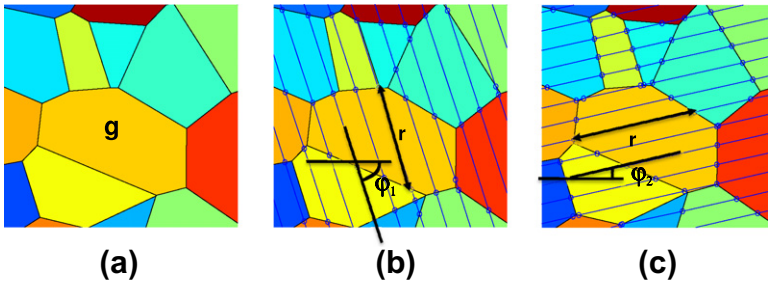

Fig. 3. Illustration of the sampling approach for GSODF: (a) for every grain orientation $\boldsymbol{g}$; the grain sizes are measured by sampling lines along various angles, as shown in (b) and (c).

crystal lattice coordinate frame): the deformation gradient $\boldsymbol{F}$ defined with respect to the initial undeformed crystal, which can be decomposed into elastic and plastic parts as $\boldsymbol{F} = \boldsymbol{F}^e\,\boldsymbol{F}^p$ (with $\det(\boldsymbol{F}^p) = 1$); the Cauchy stress $\boldsymbol{\sigma}$; and the slip resistances $s^\alpha > 0$. In the constitutive equations to be defined below, the Green elastic strain measure $\boldsymbol{E}^e = \frac{1}{2}\left(\boldsymbol{F}^{eT}\boldsymbol{F}^e - \boldsymbol{I}\right)$ defined on the relaxed configuration (plastically deformed, unstressed configuration) is utilized. The conjugate stress measure is then defined as $\boldsymbol{T} = \det\boldsymbol{F}^e(\boldsymbol{F}^e)^{-1}\,\boldsymbol{\sigma}(\boldsymbol{F}^e)^{-T}$.

The constitutive relation, for stress, is given by $\boldsymbol{T} = L^e[\boldsymbol{E}^e]$, where $\mathscr{L}^e$ is the fourth-order anisotropic elasticity tensor. It is assumed that deformation takes place through dislocation glide, and the evolution of the plastic velocity gradient is given by:

$$\boldsymbol{L}^p = \dot{\boldsymbol{F}}^p(\boldsymbol{F}^p)^{-1} = \sum_\alpha \dot{\gamma}^\alpha \boldsymbol{S}_0^\alpha sign(\tau^\alpha) \tag{9}$$

where $\boldsymbol{S}_0^\alpha = \boldsymbol{m}_0^\alpha \otimes \boldsymbol{n}_0^\alpha$ is the Schmid tensor and $\dot{\gamma}^\alpha$ is the plastic shearing rate on the α^{th} slip system. The resolved stress on the α^{th} slip system is given by $\tau^\alpha = \boldsymbol{T}\cdot\boldsymbol{S}_0^\alpha$. The shearing rate on slip systems is given by a power law:

$$\dot{\gamma}^\alpha = \dot{\gamma}^0\left|\frac{\tau^\alpha}{s^\alpha}\right|^{1/m} sign(\tau^\alpha) \tag{10}$$

where m is the strain rate sensitivity and $\dot{\gamma}^0$ is a reference rate of shearing. The evolution of slip system resistance is given by the following expression [7]:

$$\dot{s}^\alpha(t) = \sum_\beta h^{\alpha\beta}\dot{\gamma}^\beta(t), \text{with } s^\alpha(0) = \left(\tau_0^\alpha + \frac{k_0^\alpha}{\sqrt{\langle D^\alpha(0)\rangle}}\right) \tag{11}$$

$$\text{where, } h^{\alpha\beta} = \left(h_o^\beta + \frac{k_1^\beta}{\sqrt{\langle D^\beta(t)\rangle}}\right)(q + (1-q)\delta^{\alpha\beta}) \times \left(1 - \frac{s^\beta(t)}{s_s^\beta}\right)^a \text{(no sum on } \beta) \tag{12}$$

Here, τ_0^α corresponds to the flow stress of slip system α of an infinitely large grain with zero plastic strain ($\gamma^\alpha = 0$) and k_0^α is the Hall–Petch constant of slip system α at zero plastic strain. The slip system hardening term ($h^{\alpha\beta}$) includes latent hardening through parameter q. In this term, h_o^β is the hardening coefficient of slip system β in an infinitely large grain, the constant k_1^β captures the dependence of the Hall–Petch coefficient on the plastic strain of slip system β and s_s^β is the saturation resistance of slip system β. Note that $\langle D^\beta(t)\rangle$ in Eq. (12) is the average grain size measured along slip direction of β^{th} slip system in the relaxed configuration (plastically deformed, unstressed configuration) at time t.

5. Computation of Jacobians

At time t during deformation, the new positions ($\boldsymbol{g}_t$) of nodes in the fundamental region mesh (M_g) are computed using the reorientation velocities $\boldsymbol{v}$ obtained from the constitutive model. The expression for $\boldsymbol{v}$ is obtained by taking a derivative of relation Eq. (3):

$$\boldsymbol{v} = \frac{1}{2} E \cdot \Omega \tag{13}$$

where $\boldsymbol{\Omega}$ is the spin tensor defined as $\boldsymbol{\Omega} = \dot{\boldsymbol{R}}^e \boldsymbol{R}^{eT}$. Here, $\boldsymbol{R}^e$ is evaluated through the polar decomposition of the elastic deformation gradient $\boldsymbol{F}^e$ as $\boldsymbol{F}^e = \boldsymbol{R}^e \boldsymbol{U}^e$. The reorientation velocity $\boldsymbol{v} = \frac{\partial \boldsymbol{g}_t}{\partial t}$ is computed at each nodal point in the mesh, and the change in orientation $\Delta \boldsymbol{g}' = \boldsymbol{g}'_t - \boldsymbol{g}'_o$ is then calculated and stored at the nodal points in the fundamental region. The Jacobian is then computed using FE shape functions as:

$$J(\boldsymbol{g}_o, t) = \det\left(\frac{\partial \boldsymbol{g}_t}{\partial \boldsymbol{g}_o}\right) \tag{14}$$

In order to retrieve the average grain sizes $\langle D^{\alpha}(t)\rangle$ at time t for use in Eq. (12), the evolution of GSDF mesh can be computed using the plastic deformation gradient (as $\boldsymbol{r}_t = \boldsymbol{F}^p(\boldsymbol{g}, t)\boldsymbol{r}_o$). However, the Jacobian in this case is simply equal to one ($J(\boldsymbol{r}_o,t|\boldsymbol{g}) = \det(\boldsymbol{F}^p(\boldsymbol{g},t)) = 1$), and from Eq. (8) the probability distribution will remain unchanged on the nodal locations during deformation. The slip direction $\boldsymbol{m}_o^{\alpha}$ in the deformed mesh relates to the direction $\boldsymbol{m}^*$ in the undeformed mesh through the equation:

$$\boldsymbol{m}^* = \boldsymbol{F}^{p^{-1}} \boldsymbol{m}_o^{\alpha} \tag{15}$$

Since the probabilities along $\boldsymbol{m}^*$ in the undeformed mesh are the same as those along $\boldsymbol{m}_o^{\alpha}$ in the deformed mesh, the average grain size at time t can be retrieved directly using the formula:

$$\langle D^{\boldsymbol{m}_o^{\alpha}}(t)\rangle = \langle D^{\boldsymbol{m}^*}(0)\rangle / |\boldsymbol{m}^*| \tag{16}$$

where $|\boldsymbol{m}^*|$(the stretch factor) is the Euclidean norm of $\boldsymbol{m}^*$. Hence, only the average grain sizes along all directions (e.g. along a unit semi-circle in two dimensions) at time $t = 0, \langle D^{\boldsymbol{m}^*}(0)\rangle$, are needed for the update procedure. In other words, the probabilities $\mathscr{P}(\boldsymbol{r}|\boldsymbol{g})$ over mesh $M_{r|g}$ need not be evolved with time. This significantly enhances the computational efficiency of the algorithm.

The average stress for the microstructure is obtained by averaging the single crystal stresses $\boldsymbol{\sigma}$ over the ODF as follows:

$$< \boldsymbol{\sigma} >= \int \boldsymbol{\sigma}(\boldsymbol{g}_t)\mathscr{A}(\boldsymbol{g}_t) d\boldsymbol{g}_t = \int \hat{\boldsymbol{\sigma}}(\boldsymbol{g}_o, t)\mathscr{A}(\boldsymbol{g}_o, t=0) d\boldsymbol{g}_o \tag{17}$$

where $\hat{\boldsymbol{\sigma}}(\boldsymbol{g}_o, t)$ is the stress ($\boldsymbol{\sigma}(\boldsymbol{g}_t) = \boldsymbol{\sigma}(\boldsymbol{g}_o + \Delta \boldsymbol{g})$) plotted over the corresponding orientation ($\boldsymbol{g}_o$) in the initial ODF mesh. From this equation, one can conclude that, if the reorientations ($\Delta \boldsymbol{g}$) and the initial texture ($\mathscr{A}(\boldsymbol{g}_o, t=0)$) are known, the average stress (or any other average property) for the polycrystal can be evaluated. A total Lagrangian approach is used where the fundamental region mesh for $\boldsymbol{g}$ remain unchanged and the reorientations are stored at the nodal points. If the reorientations are used to move the nodal locations of the ODF grid, new orientation spaces are obtained, which are also valid fundamental regions [20]. Several ideas from the FE community were used to solve the GSODF evolution problem. For example, linear shape functions are used to interpolate the probabilities and calculate the Jacobians. Integrations are performed using Gauss points to compute integrals (such as Eq. (17)), interpolations are performed using shape functions to transfer reorientations from nodes to integration points and smoothing is performed to transfer the computed Jacobians from integration points to nodes. The overall algorithm for the GSODF update is given in Table 1.

6. Numerical examples

The deformation response predicted by the GSODF-based method has been quantified through deformation analysis of a planar polycrystalline microstructure. The following parameters were used in the power law: $\dot{\gamma}^0 = 0.001\ \mathrm{s}^{-1}$ and $m = 0.012$. A specific crystal geometry with two slip systems at orientations $-\pi/6$ and $+\pi/6$ is considered. This model leads to continuity in both reorientation velocity (v) and its gradient (∇v) over the orientation space as demonstrated by Kumar and Dawson [21]. The imposed macroscopic velocity gradient $\boldsymbol{L}$ is given as:

$$\boldsymbol{L} = \dot{\boldsymbol{F}}\boldsymbol{F}^{-1} = \eta \begin{bmatrix} 1 & 0 \\ 0 & -1 \end{bmatrix} \tag{18}$$

Here η is a constant strain rate, taken to be 0.01 for tensile and -0.01 for compressive loading. The elastic constants are taken to be $c_{11} = 2$ GPa and $c_{12} = c_{44} = 1$ GPa. The parameters in the hardening law are taken to be as follows: $\tau_0^{\alpha} = 10$ MPa, $k_0^{\alpha} = 30$ MPa $\sqrt{\mathrm{mm}}$, $h_o^{\alpha} = 10$ MPa, $k_1^{\alpha} = 10$ MPa $\sqrt{\mathrm{mm}}$, $s_s^{\alpha} = 200$ MPa, $q = 1.4$ and $a = 2$.

The GSODF of a given microstructure is obtained by sampling it using 200 lines each at 50 different angles from -90 to $+90°$. The grain size histogram, for one grain along a particular sampling direction, is obtained by measuring the intercept lengths ($\boldsymbol{r}$, as illustrated in Fig. 3). Histograms for grains that have orientations close to the nodal points in the M_g mesh (within an error of $\pm\delta\boldsymbol{g}$, $\delta\boldsymbol{g} = 0.2$ rad being a smoothing parameter) are used for computing the GSODF. The GSODF probabilities are then computed by normalizing the measured histograms.

The stress–strain response and texture evolution predicted by the GSODF algorithm in Table 1 was compared against two different approaches. In the first approach, called the "Taylor aggregate model", each grain was imposed with the same macroscopic deformation gradient, and the stresses and reorientations are tracked within each individual grain. In the second model, the crystal plasticity finite element (CPFE) model, the deformation gradient was

Table 1
Algorithm for GSODF evolution

(1) Initialize mesh M_g and load probabilities $\mathscr{A}(g)$ and average grain sizes as a function of sampling angle $\langle D^{\alpha}(\boldsymbol{g},t=0)\rangle$ computed from the sampling algorithm.
(2) Apply time increment Δt and compute the current deformation gradient $\boldsymbol{F}$ (at $t=0$, $\boldsymbol{F}=\boldsymbol{F}^e=\boldsymbol{F}^p=\boldsymbol{I}$, where $\boldsymbol{I}$ is the identity tensor).
(3) Update probabilities
  (3.1) Compute the stretch along the slip directions using Eq. (15).
  (3.2) Compute and store $\langle D^{\boldsymbol{m}_0^{\alpha}}(t)\rangle$ using Eq. (16).
  (3.3) Call constitutive model to compute stresses and reorientation velocities at nodes in the fundamental region.
  (3.4) Compute the Jacobian using Eq. (14) and update the ODF using Eq. (6).
  (3.5) Compute the average stress using Eq. (17).
(4) Go to step (2) if time $t < t_{final}$.

enforced on the external boundaries and intragranular strains were computed through FE analysis [27]. In both the Taylor aggregate and CPFE models, the GSDF is sampled separately for every individual grain, while the average grain sizes are evolved in a way similar to the GSODF model (using Eqs. (15) and (16)). Note that in the CPFE model each grain has an inhomogeneous distribution of plastic strains, so a grain-averaged plastic deformation gradient was computed for use in Eq. (15).

In the GSODF model, the GSDF is computed for each orientation (rather than for each individual grain as in the Taylor aggregate or CPFE model). In other words, two grains of the same orientation but with different grain shapes will be represented using the same averaged grain size distribution function. In the case of microstructures with constant grain shapes/sizes, the GSODF model contains the same information as the Taylor aggregate model. In this case, the GSODF algorithm must give the same stress–strain curve or texture evolution as the Taylor aggregate model. Thus, to test the algorithm, a representative volume element (RVE) of size $10 \times 10\,\mathrm{mm}^2$ containing 81 equally sized square grains was considered (shown in Fig. 4a). The initial orientations were randomly assigned and the corresponding ODF is shown in Fig. 4b. The initial ODF corresponds to an FE grid with nine line elements (and 10 nodes) in the fundamental region $(-\pi/2,\ \pi/2)$. The GSDF corresponding to node 5 of the ODF mesh is also indicated. For a square grain, there is only one possible intercept length along the horizontal and vertical directions, whereas a variety of intercept lengths are possible along other directions. Thus, the resulting GSDF in Fig. 4c shows a sharp peak at 0 and $\pm$ 90° angles at an intercept length of 1.11 mm (which corresponds to the side-length of the square grain).

The stress–strain responses predicted by the three methods for this microstructure are indicated in Fig. 5a. The GSODF and Taylor aggregate models give the same response, as expected. The FE approach (with each grain modeled as a four-noded quadrilateral element) gives a softer response since it is less constrained than the Taylor model. The texture evolution for a grain initially oriented at 70° is also shown. The overall stress–strain response predicted by the GSODF and FEM approaches are directly compared in Fig. 5c and d and show good correlation. In the case of the GSODF model, the stress contour (in Fig. 5c) is obtained based on the stresses predicted for each grain orientation in the ODF mesh. Unlike GSODF model that assumes all grains have the same deformation gradient (Taylor model), the CPFE model explicitly takes into account equilibrium across grain boundaries and leads to inhomogeneity in the evolution of grain shapes, as seen in Fig. 5d. In this example, a uniformly discretized fundamental region was sufficient to represent the smooth ODF. However, when one considers sharply textured specimens, non-uniform discretizations have to be used where the node density is increased adaptively around dominant orientations in the microstructure. A L^2 norm error of the difference between the sampled probability distribution and FE interpolated probability distribution (e.g. Ref. [28]) may be used as a convergence measure when adaptively meshing the probability spaces.

With the validity of the GSODF model established, we investigated three different microstructural effects related to GSDFs: (i) the effect of the initial grain shape; (ii) the effect of the initial grain size (Hall–Petch effect); and (iii) the effect of the time evolution of the grain shapes/sizes on the overall stress–strain response. The effect of the initial grain shape is modeled by altering the aspect ratio of the square grains. The aspect ratio (L_x/L_y) is defined as the ratio of lengths (L_x, L_y) of individual grains in the x- and y-directions. The area of the grain itself is kept constant during the study, which ensures that the initial texture is the same for all the aspect ratios investigated. Fig. 6a reveals the relationship between the yield stress and the logarithm of the grain aspect ratio. The predicted stress is at a minimum for square grains (aspect ratio of one) and increases as the grain aspect ratio changes following a parabolic relationship. The effect of the grain size (Hall–Petch effect) is shown in Fig. 6b. In this case, the grain size (L_x) of the square grains is increased while the grain orientation (texture) is kept unchanged. The relationship of the logarithm of the yield stress and the logarithm of the grain size shows a slope close to -0.5, as expected from the Hall–Petch relationship.

The results in Fig. 7 indicate the important roles of the initial grain size and shape on the stress–strain response. In addition to the effects of the initial grain size and shape, the effects of the changes in grain size and shape during loading were also investigated. In the first case, the evolution of the GSDF during deformation was switched off. This ensures that Eq. (12) only uses the initial grain size to predict the stresses during loading. In the second case, GSDF evolution is included, and the updated grain size computed at each time step is employed in Eq. (12). The stress–strain response from the two cases are shown in Fig. 7. The

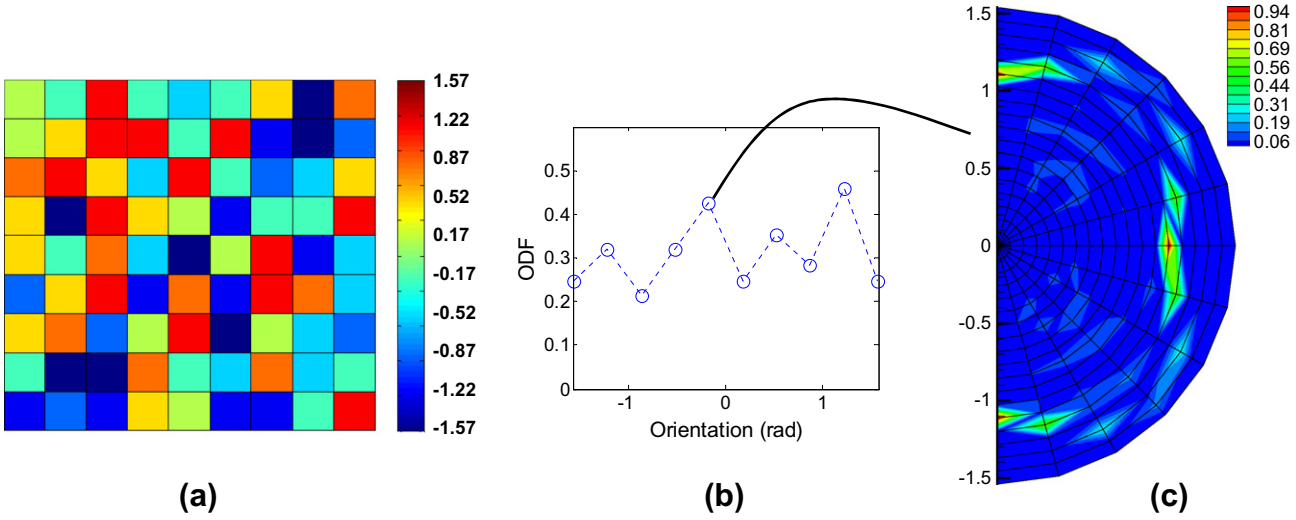

Fig. 4. (a) The initial microstructure with square grain shapes colored by grain orientation. (b) The ODF. (c) The GSDF at node $g = 0.1745$.

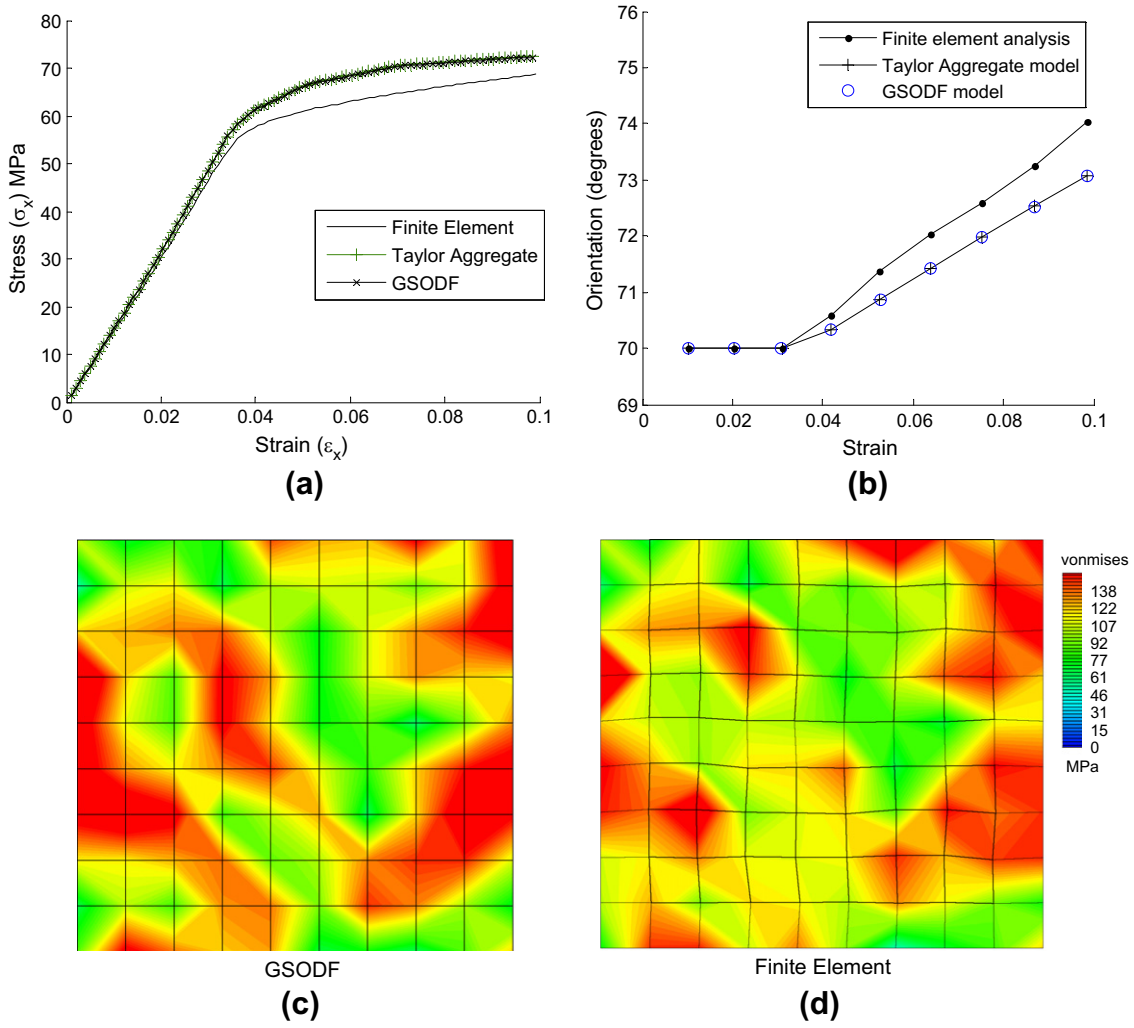

Fig. 5. (a) Comparison of the stress–strain responses for uniaxial tension predicted by the FE, Taylor aggregate and GSODF models. (b) Evolution of crystal orientation predicted by GSODF and FE analysis (for a crystal initially oriented at 70°). (c and d) Comparison of the Von Mises stress distribution predicted by the GSODF and FE models.

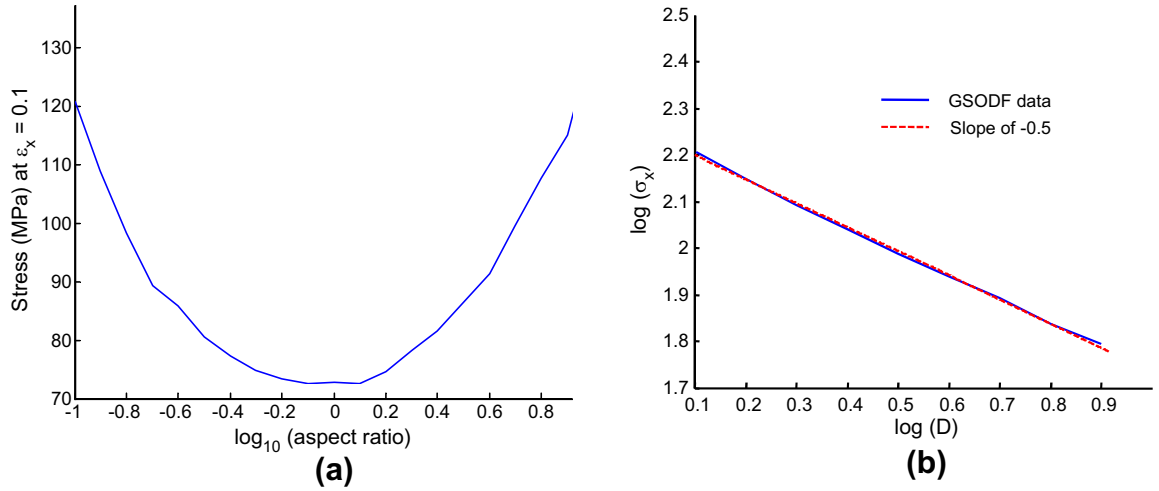

Fig. 6. (a) Variation in stress (σ_x) as a function of the aspect ratio of grains (while the ODF is kept unchanged). (b) Variation in stress with grain size (Hall–Petch relation) on a logarithmic scale.

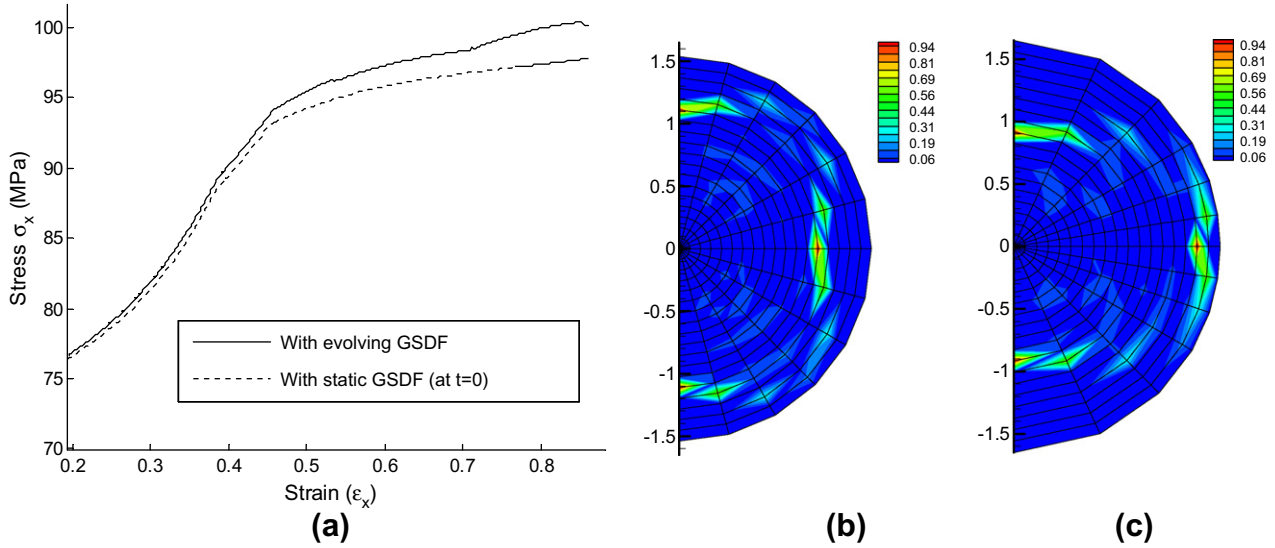

Fig. 7. (a) Comparison of the stress–strain profile predicted using only the initial GSDF with the one predicted when the GSDF is evolved with time. (b) The GSDF at orientation $\boldsymbol{g} = 0.1745$ at $t = 0$. (c) The evolved GSDF at $t = 27$ s.

stress–strain response predicted using only the initial GSDF is softer than the one predicted when the GSDF evolved with time. However, the difference is less apparent at smaller strains and is significant only at larger strain levels. The GSDF at orientation $\boldsymbol{g} = 0.1745$ at $t = 0$ and the evolved GSDF at $t = 27$ s are also shown in Fig. 7b and c respectively. The GSDF at $t = 27$ s clearly shows the lengthening of grains along the x-direction during tensile loading.

The above studies using a square-grained microstructure indicate that the effects of both initial grain shape and grain size are quite important for crystal plasticity models. On the other hand, the evolution of GSDF itself does not significantly affect the initial yield stress but may become a consideration at large strain levels. As explained previously, the GSODF model includes grain size information for each orientation (rather than each individual grain, as is the case in the Taylor and CPFE models). This leads to a significant loss of information when considering bimodal grain size distributions. Consider the microstructure shown in Fig. 8a, which includes both high and low aspect ratio grains.[1] The overall GSDF for orientation $\boldsymbol{g} = 0.1745$, shown in Fig. 8b, averages out the contribution of the different grain shapes. In order to effectively model such microstructures, an adaptive approach is suggested whereby the overall GSODF is split into two different GSODFs, one for high aspect ratio grains and another for low aspect ratio grains. In Fig. 8c, the GSDF of only

[1] The microstructure was generated using Voronoi tessellation [27]. The edges in the microstructure were not cropped to ensure that the GSDF line sampling is unbiased.

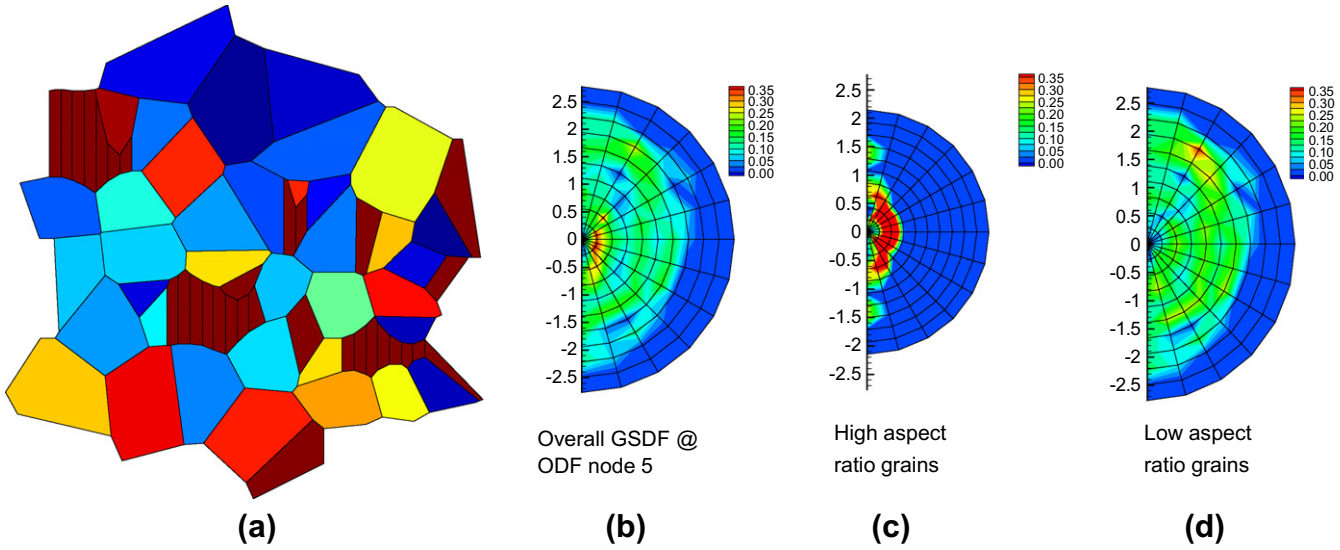

Fig. 8. (a) Initial microstructure with bimodal grain distribution. High aspect ratio grains ($L_{max}/L_{min} > 2.8$) are colored dark brown. (b) Initial GSDF at $\boldsymbol{g} = 0.1745$. (c) The GSDF of high aspect grains. (d) The GSDF of all other grains at $\boldsymbol{g} = 0.1745$. (For interpretation of the references to color in this figure legend, the reader is referred to the web version of this article.)

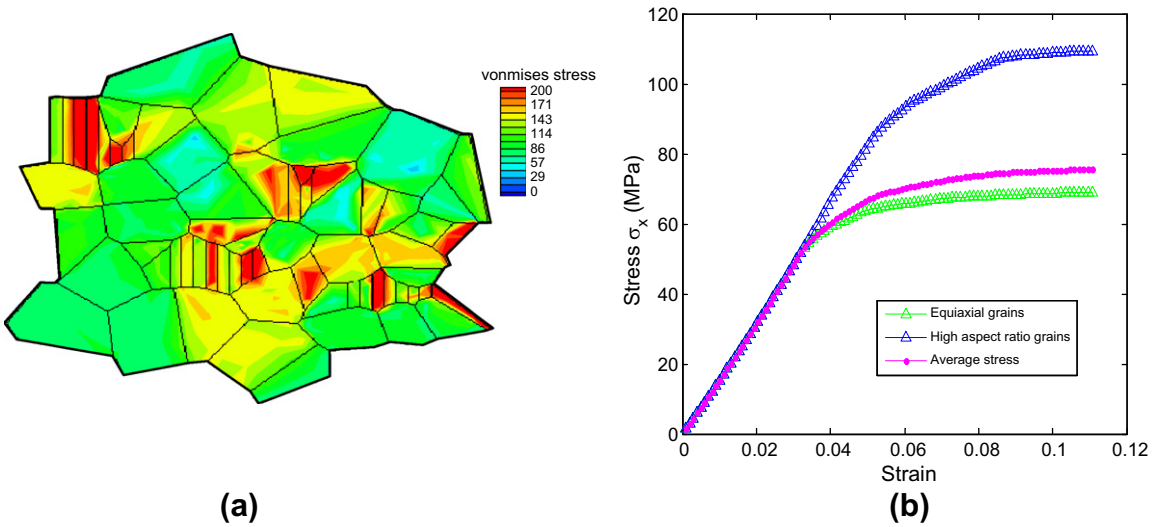

Fig. 9. (a) Von Mises stress distribution of the microstructure shows higher stresses in the high aspect ratio grains (b). Difference between the stress–strain response of high aspect ratio grains and equiaxial grains from GSODF model. The average stress–strain response of the aggregate is also shown.

the high aspect ratio grains (with $L_{max}/L_{min} > 2.8$) is shown. The GSDF of low aspect ratio grains is shown in Fig. 8d. In the adaptive approach, two independent simulations are performed: one with GSODF for low aspect ratio grains and another with GSODF for high aspect ratio grains. The results from the two different GSODF simulations are averaged based on the corresponding volume fractions to obtain the overall stress for the microstructure ($<\boldsymbol{\sigma}>$) as follows:

$$< \boldsymbol{\sigma} >=< \boldsymbol{\sigma}^H > v_f^H + < \boldsymbol{\sigma}^L > \left(1 - v_f^H\right) \tag{19}$$

where $<\boldsymbol{\sigma}^H>$ and $<\boldsymbol{\sigma}^L>$ are the average stresses predicted by the GSODF models for the high and low aspect ratio grains, respectively, and v_f^H is the volume fraction of the high aspect ratio grains in the microstructure. The adaptive GSODF model is also well suited to solving microstructures with multiple phases; for example, the high aspect ratio grains may constitute beta phase grains in an alpha–beta titanium alloy microstructure.

FE simulation for the microstructure reveals high stresses in high aspect ratio grains, as seen in Fig. 9a. The stress–strain response of these high aspect ratio grains as predicted by the GSODF model is shown in Fig. 9b. As seen from this figure, the stresses in the high aspect ratio grains are significantly larger than the low aspect ratio (equiaxed) grains. The averaged stress–strain response of the aggregate is also shown, which is calculated based on Eq. (19). A comparison of the results from an average GSODF model vs. the adaptive GSODF model and the

Taylor aggregate model is shown in Fig. 10a. In the elastic regime, all three models give the same response. However, as expected, the results from the adaptive GSODF model are closer to the stress response predicted by the Taylor aggregate model in the plastic regime. The response for a cyclic loading case is also shown in Fig. 10b. Here, one complete deformation cycle, with tension for 0.9 s followed by compression for 1.8 s and tension for another 1.8 s, is simulated. The adaptive GSODF model is seen to more closely follow the response predicted by the Taylor aggregate model.

The texture predicted by the GSODF model for the high aspect ratio grains at a strain of $\epsilon_x = 0.1$ is shown in Fig. 11a. From Ref. [21], it is seen that texture from tension process leads to an orientation sink at zero degrees and source at $\pm\pi/2$, with the basin of the sink spanning all of the orientation space. Thus, the ODF will evolve exponentially with strain and eventually approach the asymptote, which is a delta function, $A(r) = \delta(r - \pi/2)$. As seen in Fig. 11a, there is tendency for crystals with angles close to the origin to reorient farther away (sink) and an associated increase in the ODF close to the ideal orientation of $\theta = \pm\pi/2$ (source), as expected. The texture evolution predicted by the GSODF models and the Taylor aggregate model for a grain initially oriented at -0.799 rad is compared in Fig. 11b. Again, an adaptive GSODF model

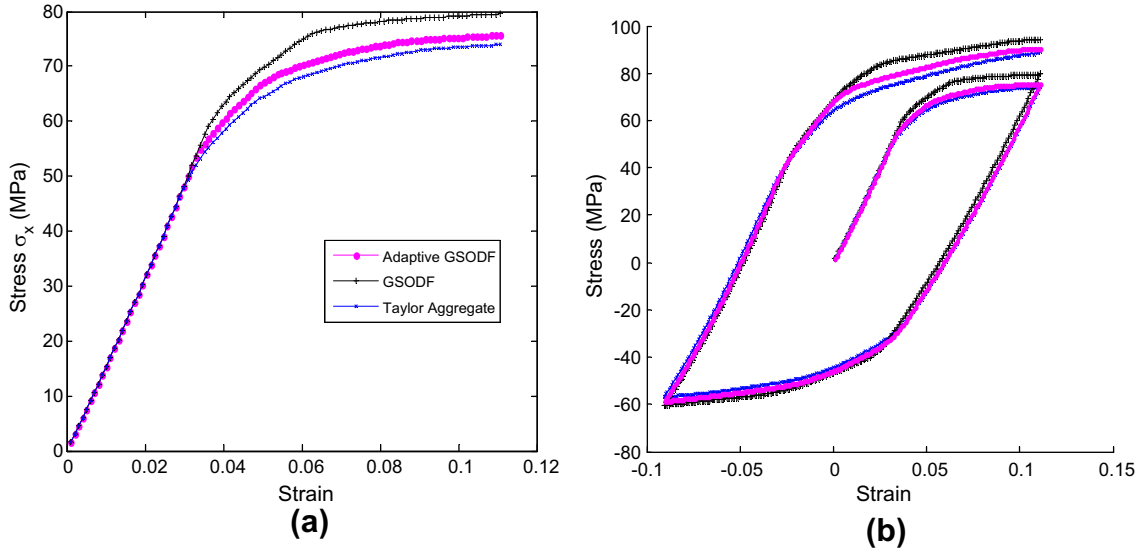

Fig. 10. (a) Comparison of stress–strain response predicted by the adaptive GSODF model against the Taylor aggregate and GSODF models. (b) Comparison of the response to cyclic deformation.

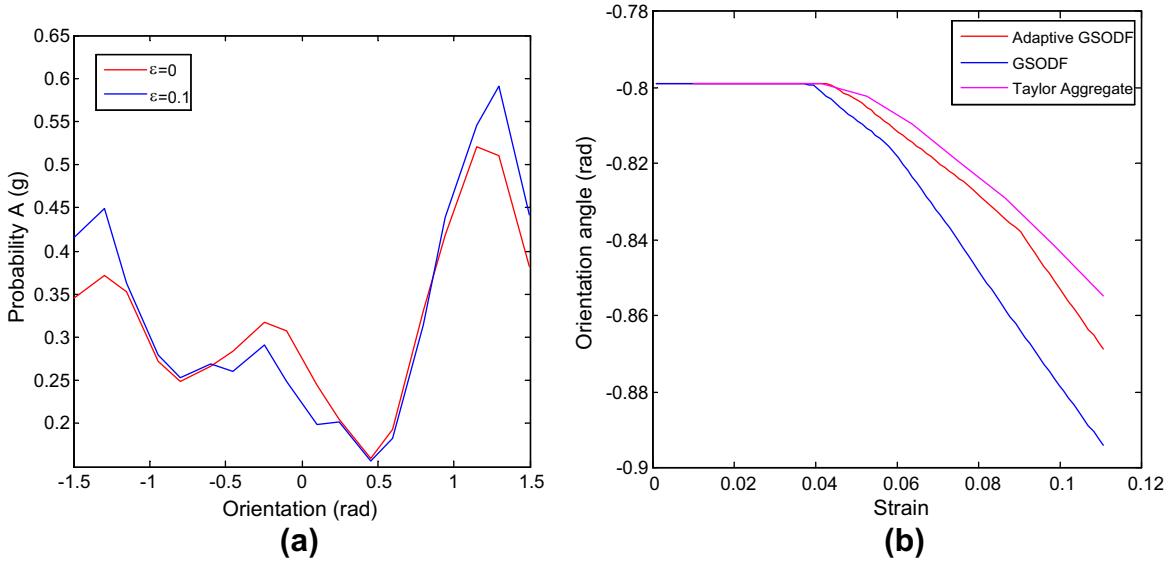

Fig. 11. (a) ODF evolution of the high aspect ratio grains. (b) Evolution of crystal orientation predicted by Taylor, GSODF and adaptive GSODF methods (for a crystal initially oriented at -0.799 rad).

results in prediction of textures that are closer to that predicted by the more computationally expensive Taylor model.

Finally, a comparison of simulation times for the CPFE, Taylor aggregate and GSODF models is shown in Fig. 12. The simulation times were computed based on the first 10 time steps ($\Delta t = 0.1$ s) of each method and normalized with respect to the simulation time for the most expensive approach (i.e. the CPFE simulation). Note that the adaptive GSODF approach uses two different GSODFs to represent the bimodal microstructure. The evolution of these GSODFs are solved as two independent problems. Consequently, the computational time is also doubled compared to a single GSODF problem. However, the net simulation time is still significantly smaller than the Taylor and FE aggregate approaches. Also, the use of two independent GSODFs to represent the bimodal microstructure implies that probabilities are not transferred across the two GSODFs when grain shapes change. This assumption is admissible within the Taylor model, where grain interactions are ignored and ultimately volume averaging is employed. However, source and sink terms in the probability spaces do need to be considered when modeling additional physics such as grain fragmentation, recrystallization and twinning. Extension of the approach to model these effects will be considered in future publications.

From Fig. 12, it is clear that probabilistic methods (GSODF or adaptive GSODF methods) are significantly faster than FE and Taylor aggregate models. This is because of the use of only a few nodes in the orientation space vs. the use of complete microstructural meshes in the case of aggregate models. The simulation time for the GSODF model is independent of the size of the RVE since the statistics are represented over the same mesh for all cases. In contrast, as the number of elements in the RVE increases, the computational expense in aggregate models increase as $O(N^2)$. Note that, in both aggregate and the models, remeshing is required at large strains. Element distortion is significantly more of an issue for aggregate models where the entire microstructure needs to be remeshed at large strains. In the case of GSODF models, the nodal points in the orientation space may begin to overlap and interpenetrate at large strains, and remeshing (of the simpler orientation space) may be needed at large strains. The total Lagrangian approach used in this work was found to be adequate up to a strain of 1.25 for the case of the square-grained microstructure.

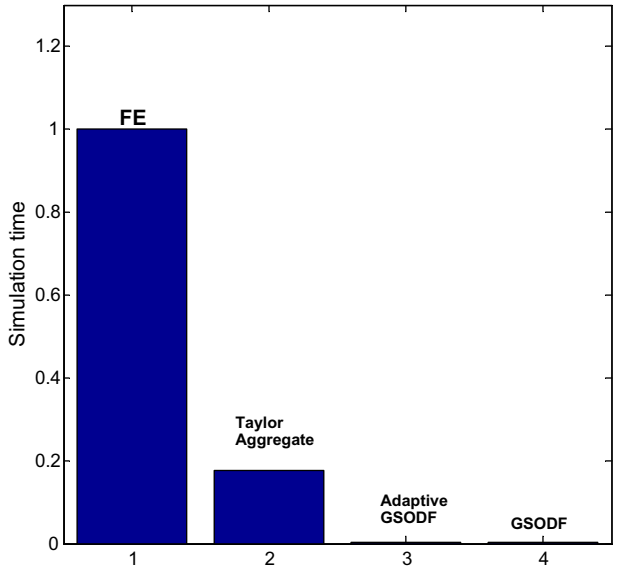

Fig. 12. Comparison of simulation times (normalized) for various methods. Probabilistic methods are significantly faster than the FE and Taylor aggregate models.

7. Conclusions and future directions

In this paper, a new statistical theory that takes into account the coupling between grain size, shape and crystallographic texture during deformation of polycrystalline microstructures was introduced. The effect of grain shape is modeled by including the apparent grain size as seen by various different active slip systems in the grain within the constitutive law for the slip resistance. The coupling between the crystallographic texture and grain shape is considered by employing the grain size orientation distribution function (GSODF), which encodes the probability density of finding a grain size D along direction $\boldsymbol{n}$ within grains of orientation g. The GSODF is sampled and represented in an FE mesh. During elastoplastic deformation, the evolution of grain size D (in direction θ) and the orientation g is tracked by directly updating the GSODF probabilities using a Lagrangian probability update scheme. The GSODF model includes grain size information for each orientation (rather than each individual grain, as in the case of the Taylor and CPFE models). The GSODF model is identical to Taylor-aggregate model if all grains have the same grain shape.

For distinctly bimodal microstructures, two GSODFs can be employed for different grain shapes, which leads to results close to the Taylor aggregate model at a fraction of the computational cost. The role of grain shape (grain aspect ratio) was investigated in the case of 2-D microstructures and was found to be a significant factor in determining the overall plastic response. The yield stress approximately followed a parabolic relationship with the logarithm of the aspect ratio of grains, with the minimum yield stress achieved in the case of a grain aspect ratio of one. The overall constitutive model reproduced the Hall–Petch effect, with the yield stress following an inverse square root relationship with the grain size. On the other hand, the evolution of the GSDF itself does not significantly affect the initial yield stress, but was found to be a consideration at large strain levels. In contrast to aggregate models (Taylor or CPFE), the simulation time for the GSODF model is significantly shorter and is independent of the size of the microstructure. The improvement in computational efficiency achieved by GSODF models is most useful when performing multiscale design of industrial

forming processes (e.g. our recent work in Ref. [29]) with bimodal or multimodal microstructures with various grain shapes. Further, the nodes in the orientation space can be adaptively refined to ensure sharp probabilities can be captured. For example, a single crystal close to a crack tip can be modeled using a GSODF which is a delta function in the orientation space. Such sharp probability distributions can be generated by refining the element sizes in the orientation space. Farther from the notch tip, the experimentally measured ODF can be modeled within a regularly spaced grid. Adaptive methods to mesh and remesh the GSODF will be a subject of future study in this area, as will be methods to extend the simulation presented here to 3-D orientation spaces (fcc, hcp) and to perform multiscale process simulations.

Acknowledgements

The work presented here was funded by Office of Naval Research (ONR) grant N00014-12-1-0013 and National Science Foundation CAREER award (CMMI-0954390). Constructive comments were gratefully received from Dr. William Mullins (ONR).

References

[1] Allison J, Backman D, Christodoulou L. J Min Met Mater Soc 2006;58:25.
[2] Hall EO. Proc Phys Soc B 1951;64:747.
[3] Petch NJ. J Iron Steel Inst 1953;174:25.
[4] Kocks UF, Tomé CN, Wenk HR. Texture and anisotropy – preferred orientations in polycrystals and their effect on materials properties. Cambridge: Cambridge University Press; 2000.
[5] Bunge HJ. Texture analysis in materials science. London: Butterworth; 1982.
[6] Armstrong R, Codd I, Douthwaite RM, Petch NJ. Philos Mag 1962;7:45.
[7] Weng GJ. J Mech Phys Solids 1983;31:193.
[8] Nicaise N, Berbenni S, Wagner F, Berveiller M, Lemoine X. Int J Plast 2011;27:232.
[9] Raeisinia B, Sinclair CW, Poole WJ, Tom CN. Modell Simulat Mater Sci Eng 2008;16:1.
[10] Shu JY, Fleck NA. J Mech Phys Solids 1999;47:297.
[11] Acharya A, Beaudoin AJ. J Mech Phys Solids 2000;48:2213.
[12] Counts WA, Braginsky MV, Battaile CC, Holm EA. Int J Plast 2008;24:1243.
[13] Evers LP, Brekelmans WAM, Geers MGD. Int J Solids Struct 2004;41:5209.
[14] Bunge HJ, Wagner F, Welch PI, van Houtte P. J Phys Lett 1985;46:L1109.
[15] Wagner F, Bunge HJ, Van Houtte P. In: Eighth international conference on textures of materials. Warrendale (PA): Metallurgical Society; 1988, p. 369.
[16] Tiem S, Berveiller M, Canova GR. Acta Metall 1986;34:2139.
[17] Taylor GI. J Inst Met 1938;62:307.
[18] Fromm BS, Adams BL, Ahmadi S, Knezevic M. Acta Mater 2009;57:2339.
[19] Sundararaghavan V, Kumar A. Int J Plast 2012;30:62.
[20] Kumar A, Dawson PR. Comput Meth Appl Mech Eng 1996;130:227.
[21] Kumar A, Dawson PR. Comput Meth Appl Mech Eng 1996;130:247.
[22] Adams BL, P Boehler J, Guidi M, Onat ET. J Mech Phys Solids 1992;40:723.
[23] Kalidindi SR, Duvvuru HK. Acta Mater 2005;53:3613.
[24] Vander Voort GF. Metallography: principles and practice. New York: McGraw-Hill; 1984.
[25] Clement A. Mater Sci Eng 1982;55:203.
[26] Asaro RJ, Needleman A. Acta Metall 1985;33:923.
[27] Sundararaghavan V, Zabaras N. Int J Plast 2006;22:1799.
[28] Zienkiewicz OC, Zhu JZ. Int J Numeric Meth Eng 1987;24:337.
[29] Sundararaghavan V, Zabaras N. Int J Plast 2008;24:1581.